Iranian Journal of Numerical Analysis and Optimization
Vol. 9, No. 2, (2019), pp 141–163
DOI:10.22067/ijnao.v9i2.77371

Research Article

A new regularization term based on second order total generalized variation for image denoising problems

E. Tavakkol, S.M. Hosseini* and A.R. Hosseini

Abstract

Variational models are one of the most efficient techniques for image denoising problems. A variational method refers to the technique of optimizing a functional in order to restore appropriate solutions from observed data that best fit the original image. This paper proposes to revisit the discrete total generalized variation (TGV) image denoising problem by redefining the operations via the inclusion of a diagonal term to reduce the staircasing effect, which is the patchy artifacts usually observed in slanted regions of the image. We propose to add an oblique scheme in discretization operators, which we claim is aware of the alleviation of the staircasing effect superior to the conventional TGV method. Numerical experiments are carried out by using the primal-dual algorithm, and numerous real-world examples are conducted to confirm that the new proposed method achieves higher quality in terms of relative error and the peak signal to noise ratio compared with the conventional TGV method.

AMS(2010): 68Q25; 68R10; 68U05.

Keywords: Image denoising; Total variation; Staircasing effect; Total generalized variation; Peak signal to noise ratio.

*Corresponding author
Received 15 December 2018; revised 13 March 2019; accepted 29 April 2019
E. Tavakkol
Department of Applied Mathematics, Tarbiat Modares University, P. O. Box 14115-175, Tehran, Iran. e-mail: e.tavakkol@modares.ac.ir

S.M. Hosseini
Department of Applied Mathematics, Tarbiat Modares University, P. O. Box 14115-175, Tehran, Iran. e-mail: hossei_m@modares.ac.ir

A.R. Hosseini
School of Mathematics, Statistics and Computer Science, College of Science, University of Tehran, P. O. Box 14115-175, Tehran, Iran. e-mail: hosseini.alireza@ut.ac.ir

1 Introduction

Digital image processing (DIP) deals with performing operations on digital images. A digital image is a numerical representation of a physical scene, which is composed of a finite number of pixels. Digital images are produced by means of imaging machines that cover the electromagnetic spectrum. Synthetic images, electron microscopy images, and ultra-sound images are examples of digital images. Digital images were first used in the newspaper industry in the 1920s. These digital images were produced from a coded tape by a telegraph printer. The field of DIP is enriched with various applications, including image restoration [3,17,23,25], artistic effects [19], medical visualization [9,27,28,30], industrial inspection [22], law enforcement [32,33], and so on. Image restoration is one of the most widespread applications of DIP techniques that implements processes on digital images in order to estimate the original image from the corrupted one. The image distortion is caused due to different types of noise, such as Gaussian noise, white noise, salt and pepper noise, and speckle noise. In recent decades, variational approaches have been used as an efficient tool for image denoising problems.

A variational model is an optimization problem in which the criterion is defined as a functional (energy), which consists of a regularization term and a data fidelity term. Total variation (TV) regularization is a variational model that uses total variation as a regularization term. TV regularization was first proposed by Rudin, Osher, and Fatemi (ROF model) for imaging problems; see [26]. The ROF method is edge-preserving and has a fast numerical algorithm. Many different papers have shown the efficiency of TV minimization for image restoration [1,4,5,8,10,11,13–15,18,20,21,24,29,31]. The TV regularization has been widely used in various applications, such as image deblurring, inpainting, image zooming, segmentation problems, interpolation, spectral extrapolation, and stereovision. In these methods, the TV semi-nom is defined as

$$TV(u) = sup \left\{ \int_{\Omega} u \; div \; \nu \; dx \;\middle|\; \nu \in C_c^1(\Omega, \mathbf{R}^n), \; ||\nu||_\infty \leq 1 \right\},$$

where u is a function defined on a bounded region $\Omega \subset \mathbf{R}^n$. TV based regularization models have been proved to be efficient in image denoising problems. However, these models suffer from the staircasing effect, which appears as undesired patchy artifacts in slanted regions (see Figure 1). The total generalized variation (TGV) regularization model [6] is one technique to overcome this shortcoming, which acts as a regularization functional that incorporates higher-order derivatives and regularizes independently on various regularity levels. The main idea of TGV is a generalization of TV, which is defined as

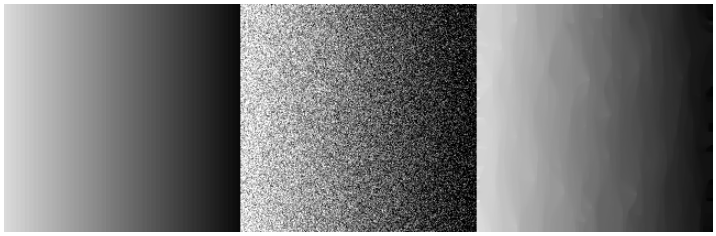

Figure 1: The implementation results of 1500 iterations of the ROF TV model [26]. From left to right: The reference image, the noisy image, and the restored image using the ROF TV. The original image has been corrupted by additive white Gaussian noise of standard deviation 0.18 and the regularization parameter is set to $\lambda = 0.17$. The ROF denoising model leads to staircasing effect, which is observed as patchy artifacts.

$$TGV_{\lambda}^{k}(u) = sup \left\{ \int_{\Omega} u \; div^{k}\nu \; dx \;\middle|\; \nu \in C_{c}^{k}(\Omega, Sym^{k}(\mathbf{R}^{n})),\; ||div^{l}\nu||_{\infty} \leq \lambda_{l}, \right.$$
$$\left. l = 0, \ldots, k-1 \right\},$$

where $k \geq 1$, $n \geq 1$, and λ_l are fixed positive parameters, and $Sym^k(\mathbf{R}^n)$ denotes the space of symmetric tensors of order k with arguments in $\mathbf{R}^n$. This paper proposes to revisit the TGV image denoising model by redefining the gradient operations via the inclusion of diagonal terms to reduce the staircasing effect. We propose to add an oblique scheme in classical image derivatives discretization, which we claim is aware of the alleviation of the staircasing effect superior to the conventional TGV method. Numerical experiments are carried out using the primal-dual algorithm, and numerous real-world experiments are conducted to confirm the effectiveness of the new approach.

The remainder of this paper is organized as follows. First, a brief explanation of some essential concepts regarding the TV and TGV schemes is presented in section 2. In section 3, the new proposed regularization model for image denoising problems and the corresponding theoretical results are presented. Section 4 is devoted to numerical experiments and comparisons that demonstrate the efficiency of the proposed method. Finally, Section 5 contains some concluding remarks.

2 Background

In this section, we present a brief review on essential concepts of TV and TGV approaches.

2.1 TV concept

Assume that u is a function defined on a bounded region $\Omega \subset \mathbf{R}^n$. The function u is said of bounded variation (BV function) if it is integrable and there exists a Radon measure Du such that

$$\int_\Omega u \; div \; \nu \; dx = - \int_\Omega \nu \; Du \; dx,$$

for all $\nu \in C_c^1(\mathbf{R}^n, \mathbf{R}^n)$, where $C_c^1(\mathbf{R}^n, \mathbf{R}^n)$ is the space of continuously differentiable vector functions ν of compact support and Du is the distributional (weak) derivative of u. The TV seminorm of u is defined as

$$TV(u) := sup\Big\{ \int_\Omega u \; div \; \nu \; dx \;\Big|\; \nu \in C_c^1(\Omega, \mathbf{R}^n), \; ||\nu||_\infty \leq 1 \Big\} = \int_\Omega |Du| dx,$$

where $|.|$ is the Euclidean norm. In the case that u is a smooth function, we have $Du = \nabla u$; therefore $TV(u)$ is the integral of its gradient magnitude

$$TV(u) = \int_\Omega |\nabla u| dx.$$

2.2 TGV concept

In this subsection, we review the essential concepts of TGV regularization from [6].

Definition 1. Let $k \geq 1$, $\Omega \subset \mathbf{R}^n$ be a bounded region, and $\lambda_0, \ldots, \lambda_{k-1}$ be fixed positive parameters. For $u \in L_{loc}^1(\Omega)$, the total generalized variation of order k with weight $\lambda \in \mathbf{R}^k$ is defined by the functional

$$TGV_\lambda^k(u) = sup \; \Big\{ \int_\Omega u \; div^k \nu \; dx \;\Big|\; \nu \in C_c^k(\Omega, Sym^k(\mathbf{R}^n)), \; ||div^l \nu||_\infty \leq \lambda_l,$$

$$l = 0, \ldots, k-1 \; \Big\},$$

where $\lambda = (\lambda_0, \ldots, \lambda_{k-1})$, $C_c^k(\Omega, Sym^k(\mathbf{R}^n))$ is the space of k-times continuously differentiable functions with compact support from Ω to $Sym^k(\mathbf{R}^n)$ and $Sym^k(\mathbf{R}^n)$ is the vector space of symmetric k-tensors defined as

$$Sym^k(\mathbf{R}^n) = \Big\{ \eta : \underbrace{\mathbf{R}^n \times \cdots \times \mathbf{R}^n}_{\text{k times}} \to \mathbf{R} \;\Big|\; \eta \; is \; k\text{-}linear \; and \; symmetric \Big\}.$$

For the case when $k = 2$, the TGV_λ^2 functional is a special case of TGV_λ^k functional, which is defined as

$$TGV_\lambda^2(u) = sup \; \Big\{ \int_\Omega u \; div^2 \nu \; dx \;\Big|\; \nu \in C_c^2(\Omega, Sym^2(\mathbf{R}^n)), \; ||\nu||_\infty \leq \lambda_0,$$

$$||div\ \nu||_\infty \leq \lambda_1\Big\}, \tag{1}$$

where $\lambda = (\lambda_0, \lambda_1)$ and

$$(div\ \nu)_i = \sum_{j=1}^{d} \frac{\partial \nu_{ij}}{\partial x_i},\ div^2\nu = \sum_{i=1}^{d} \frac{\partial^2 \nu_{ii}}{\partial x_i^2} + 2\sum_{i<j} \frac{\partial \nu_{ij}}{\partial x_i \partial x_j}.$$

Remark 1. The Euclidean space $\mathbf{R}^{N_1\times N_2}$ is equipped with the inner product

$$\langle u, s\rangle_{\mathbf{R}^{N_1\times N_2}} = \sum_{i=1}^{N_1}\sum_{j=1}^{N_2} u_{i,j}s_{i,j}, \quad u, s \in \mathbf{R}^{N_1\times N_2}.$$

For $u \in \mathbf{R}^{N_1\times N_2}$, the second order TGV semi-norm (1) can be discretized as

$$TGV_\lambda^2(u) = \max\ \Big\{\langle u, div^2\nu\rangle_{\mathbf{R}^{N_1\times N_2}} \ \Big|\ \nu \in (\mathbf{R}^4)^{N_1\times N_2},\ \nu = \begin{pmatrix} \nu_{11} & \nu_{12} \\ \nu_{12} & \nu_{22} \end{pmatrix},$$

$$\nu_{ij} \in \mathbf{R}^{N_1\times N_2}\ (i,j=1,2),\ ||\nu||_\infty \leq \lambda_0, ||div\ \nu||_\infty \leq \lambda_1\Big\}, \tag{2}$$

where $\lambda = (\lambda_0, \lambda_1)$. The discrete version of the infinity norm for the vector field z, where $z = div\ \nu$, is defined as

$$||z||_\infty = sup\left\{ \left(\sum_{i=1}^{n} z_i(x)^2 \right)^{1/2} \ \Big|\ x \in \Omega \right\}.$$

Moreover, the discrete version of the infinity norm for matrix ν is defined as

$$||\nu||_\infty = sup\left\{ \left(\sum_{i=1}^{n} \nu_{ii}(x)^2 + 2\sum_{i<j} \nu_{ij}(x)^2 \right)^{1/2} \ \Big|\ x \in \Omega \right\}.$$

3 The new proposed method

In this section, we present a new variant of the TGV model for the alleviation of the staircasing effect in image denoising problems by redefining the operators via the inclusion of a diagonal term. In the conventional TGV model presented in [6], the discretization operators are based on finite differences in the direction of the horizontal and vertical axes. Here, we reconstruct the discretization operators in [6] via the inclusion of a diagonal term. For this purpose, we introduce the versions of the discretization operators in parts (**a**-**e**). The indexes x, y, and o indicate that the corresponding finite-differences

are established in the direction of the horizontal, vertical, and diagonal axis, respectively.

a. For $u \in \mathbf{R}^{N_1 \times N_2}$, we define the discretization operator $\delta : \mathbf{R}^{N_1 \times N_2} \longrightarrow (\mathbf{R}^3)^{N_1 \times N_2}$ as

$$\delta(u) = \begin{bmatrix} \partial_x^+(u) \\ \partial_y^+(u) \\ \partial_o^+(u) \end{bmatrix},$$

$(i = 1, \ldots, N_1,\ j = 1, \ldots, N_2)$, where

$$(\partial_x^+ u)_{i,j} = \begin{cases} u_{i+1,j} - u_{i,j} & \text{if } \ 1 \le i < N_1, \\ 0 & \text{if } \ i = N_1, \end{cases}$$

$$(\partial_y^+ u)_{i,j} = \begin{cases} u_{i,j+1} - u_{i,j} & \text{if } \ 1 \le j < N_2, \\ 0 & \text{if } \ j = N_2, \end{cases}$$

$$(\partial_o^+ u)_{i,j} = \begin{cases} u_{i+1,j+1} - u_{i,j} & \text{if } \ 1 \le i < N_1, 1 \le j < N_2, \\ 0 & \text{if } \ i = N_1, j = N_2. \end{cases}$$

b. For $p = \begin{bmatrix} p_1 \\ p_2 \\ p_3 \end{bmatrix}$, $p_i \in \mathbf{R}^{N_1 \times N_2}$ $(i = 1, 2, 3)$, the discretization operator $\zeta : (\mathbf{R}^3)^{N_1 \times N_2} \longrightarrow \mathbf{R}^{N_1 \times N_2}$ is defined as

$$\zeta(p) = \partial_x^-(p_1) + \partial_y^-(p_2) + \partial_o^-(p_3),$$

where

$$(\partial_x^- p_1)_{i,j} = \begin{cases} (p_1)_{i,j} - (p_1)_{i-1,j} & \text{if } \ 1 < i < N_1, \\ (p_1)_{i,j} & \text{if } \ i = 1, \\ -(p_1)_{i-1,j} & \text{if } \ i = N_1, \end{cases}$$

$$(\partial_y^- p_2)_{i,j} = \begin{cases} (p_2)_{i,j} - (p_2)_{i,j-1} & \text{if } \ 1 < j < N_2, \\ (p_2)_{i,j} & \text{if } \ j = 1, \\ -(p_2)_{i,j-1} & \text{if } \ j = N_2, \end{cases}$$

$$(\partial_o^- p_3)_{i,j} = \begin{cases} (p_3)_{i,j} - (p_3)_{i-1,j-1} & \text{if } \ 1 < i \le N_1, 1 < j \le N_2, \\ (p_3)_{i,j} & \text{if } \ i = 1, j = 1. \end{cases}$$

c. For $p = \begin{bmatrix} p_1 \\ p_2 \\ p_3 \end{bmatrix}$, $p_i \in \mathbf{R}^{N_1 \times N_2}$ $(i = 1, 2, 3)$, the discretization operator $\xi : (\mathbf{R}^3)^{N_1 \times N_2} \longrightarrow (\mathbf{R}^9)^{N_1 \times N_2}$ is defined as

$$\xi(p) = \begin{bmatrix} \partial_x^-(p_1) & \frac{1}{2}(\partial_x^-(p_2) + \partial_y^-(p_1)) & \frac{1}{2}(\partial_x^-(p_3) + \partial_o^-(p_1)) \\ \frac{1}{2}(\partial_x^-(p_2) + \partial_y^-(p_1)) & \partial_y^-(p_2) & \frac{1}{2}(\partial_y^-(p_3) + \partial_o^-(p_2)) \\ \frac{1}{2}(\partial_x^-(p_3) + \partial_o^-(p_1)) & \frac{1}{2}(\partial_y^-(p_3) + \partial_o^-(p_2)) & \partial_o^-(p_3) \end{bmatrix},$$

where ∂_x^-, ∂_y^-, and ∂_o^- are defined as in part (**b**).

d. For $\nu = \begin{bmatrix} \nu_{11}\ \nu_{12}\ \nu_{13} \\ \nu_{12}\ \nu_{22}\ \nu_{23} \\ \nu_{13}\ \nu_{23}\ \nu_{33} \end{bmatrix}$, $\nu_{ij} \in \mathbf{R}^{N_1 \times N_2}$ $(i,j = 1,2,3)$, the discretization operator $\zeta : (\mathbf{R}^9)^{N_1 \times N_2} \longrightarrow (\mathbf{R}^3)^{N_1 \times N_2}$ is defined as

$$\zeta(\nu) = \begin{bmatrix} \partial_x^+(\nu_{11}) + \partial_y^+(\nu_{12}) + \partial_o^+(\nu_{13}) \\ \partial_x^+(\nu_{12}) + \partial_y^+(\nu_{22}) + \partial_o^+(\nu_{23}) \\ \partial_x^+(\nu_{13}) + \partial_y^+(\nu_{23}) + \partial_o^+(\nu_{33}) \end{bmatrix},$$

where ∂_x^+, ∂_y^+, and ∂_o^+ are defined as in part (**a**).

e. For $\nu = \begin{bmatrix} \nu_{11}\ \nu_{12}\ \nu_{13} \\ \nu_{12}\ \nu_{22}\ \nu_{23} \\ \nu_{13}\ \nu_{23}\ \nu_{33} \end{bmatrix}$, $\nu_{ij} \in \mathbf{R}^{N_1 \times N_2}$ $(i,j = 1,2,3)$, the discretization operator $\zeta^2 : (\mathbf{R}^9)^{N_1 \times N_2} \longrightarrow \mathbf{R}^{N_1 \times N_2}$ is defined as

$$\zeta^2(\nu) = \partial_x^-\partial_x^+(\nu_{11}) + \partial_y^-\partial_y^+(\nu_{22}) + \partial_o^-\partial_o^+(\nu_{33}) + \partial_x^-\partial_y^+(\nu_{12}) + \partial_x^-\partial_o^+(\nu_{13})$$
$$+\partial_y^-\partial_x^+(\nu_{12}) + \partial_y^-\partial_o^+(\nu_{23}) + \partial_o^-\partial_x^+(\nu_{13}) + \partial_o^-\partial_y^+(\nu_{23}).$$

where ∂_x^+, ∂_y^+, ∂_o^+, ∂_x^-, ∂_y^-, and ∂_o^- are defined as in parts (**a**) and (**b**).

The next step, we aim to solve the following variational image denoising problem

$$\min_u\ \tfrac{1}{2}||u - u_0||_2^2 + L_\lambda(u), \tag{3}$$

where $u_0 \in \mathbf{R}^{N_1 \times N_2}$ is the noisy image, $u \in \mathbf{R}^{N_1 \times N_2}$ is the image to be reconstructed, $\lambda = (\lambda_0, \lambda_1)$ (λ_0, λ_1 are the regularization parameters), and $L_\lambda(u)$ is the new proposed regularization functional, which is defined as

$$L_\lambda(u) = \max\ \Big\{ \langle u\ ,\ \zeta^2(\nu) \rangle_{\mathbf{R}^{N_1 \times N_2}} \ \Big|\ \nu \in (\mathbf{R}^9)^{N_1 \times N_2},\ \nu = \begin{bmatrix} \nu_{11}\ \nu_{12}\ \nu_{13} \\ \nu_{12}\ \nu_{22}\ \nu_{23} \\ \nu_{13}\ \nu_{23}\ \nu_{33} \end{bmatrix},$$
$$\nu_{i,j} \in \mathbf{R}^{N_1 \times N_2}\ (i,j = 1,2,3),\ ||\nu||_\infty \le \lambda_0,\ ||\zeta(\nu)||_\infty \le \lambda_1 \Big\}. \tag{4}$$

3.1 Theoretical results

We apply the over-relaxed Chambolle–Pock algorithm described in [16] for solving (3). Since this algorithm solves jointly the primal and dual formulations of minimization problem (3), we need to obtain the Fenchel dual formulation of functional (4). The analytical process for establishing this formulation of (4) is stated in Theorem 2, in which we follow the steps of [7] for its proof. Before studying this theorem, the reader needs to be familiar with the concept of Legendre–Fenchel duality and Fenchel duality theorem from [2].

Definition 2. Given some convex, proper, and lower semi-continuous function $f(p)$ defined for $p \in H$, where H is a Hilbert space with inner product $\langle ., . \rangle_H$, its Legendre–Fenchel dual function is defined as

$$f^*(q) = \max \{ \langle p, q \rangle_H - f(p) \Big| p \in H \}$$

for all $q \in H$.

Theorem 1. *Assume that X and Y are real Banach spaces, that $f_1 : X \longrightarrow (-\infty, +\infty)$ and $f_2 : Y \longrightarrow (-\infty, +\infty)$ are proper, convex, and lower semi-continuous functions, and that $A : X \longrightarrow Y$ is a linear continuous operator. If there exists $x_0 \in X$ such that $f_1(x_0) < \infty$ and f_2 is continuous at Ax_0, then*

$$\min \{ f_1(x) + f_2(A(x)) \Big| x \in X \} = \max \{ -f_2^*(y^*) - f_1^*(-A^* y^*) \Big| y^* \in Y^* \}.$$

Remark 2. For $p = \begin{bmatrix} p_1 \\ p_2 \\ p_3 \end{bmatrix} \in (\mathbf{R}^3)^{N_1 \times N_2}$ and $w = \begin{bmatrix} w_1 \\ w_2 \\ w_3 \end{bmatrix} \in (\mathbf{R}^3)^{N_1 \times N_2}$, the Euclidean space $(\mathbf{R}^3)^{N_1 \times N_2}$ is equipped with the inner product

$$\langle p, w \rangle_{(\mathbf{R}^3)^{N_1 \times N_2}} = \sum_{i=1}^{N_1} \sum_{j=1}^{N_2} (p_1)_{i,j} (w_1)_{i,j} + (p_2)_{i,j} (w_2)_{i,j} + (p_3)_{i,j} (w_3)_{i,j}.$$

Theorem 2. *The discrete second order total generalized variation functional (4) is equivalent to the following Fenchel dual formulation*

$$\begin{aligned} L_\lambda(u) = \min \ & \lambda_0 ||\xi(p)||_1 + \lambda_1 ||\delta(u) - p||_1, \\ & p \in (\boldsymbol{R}^3)^{N_1 \times N_2}, \end{aligned}$$

where ξ and δ are defined as in parts $(\boldsymbol{c})$ and $(\boldsymbol{a})$, respectively.

Proof. We prove in the lines of [7]. Based on (4), we have

$$L_\lambda(u) = \max\left\{ \langle u, \zeta^2(\nu)\rangle_{\mathbf{R}^{N_1\times N_2}} \;\middle|\; \nu \in (\mathbf{R}^9)^{N_1\times N_2},\ ||\nu||_\infty \le \lambda_0,\ ||\zeta(\nu)||_\infty \le \lambda_1 \right\}$$
$$= \max\left\{ \langle u, \zeta^2(\nu)\rangle_{\mathbf{R}^{N_1\times N_2}} - I_{\{||.||_\infty \le \lambda_0\}}(\nu) - I_{\{||.||_\infty \le \lambda_1\}}(\zeta(\nu)) \;\middle|\; \nu \in (\mathbf{R}^9)^{N_1\times N_2} \right\}$$
$$= -\min\left\{ I_{\{||.||_\infty \le \lambda_0\}}(\nu) + I_{\{||.||_\infty \le \lambda_1\}}(\zeta(\nu)) - \langle u, \zeta^2(\nu)\rangle_{\mathbf{R}^{N_1\times N_2}} \;\middle|\; \nu \in (\mathbf{R}^9)^{N_1\times N_2} \right\},$$

where

$$I_{\{||.||_\infty \le \lambda_0\}}(\nu) = \begin{cases} 0 & \text{if } ||\nu||_\infty \le \lambda_0, \\ \infty & \text{if } ||\nu||_\infty > \lambda_0, \end{cases}$$

$$I_{\{||.||_\infty \le \lambda_1\}}(\zeta(\nu)) = \begin{cases} 0 & \text{if } ||(\zeta(\nu))||_\infty \le \lambda_1, \\ \infty & \text{if } ||(\zeta(\nu))||_\infty > \lambda_1. \end{cases}$$

We choose

$$f_1(\nu) = I_{\{||.||_\infty \le \lambda_0\}}(\nu),\ f_2(\zeta(\nu)) = I_{\{||.||_\infty \le \lambda_1\}}(\zeta(\nu)) - \langle u, \zeta^2(\nu)\rangle_{\mathbf{R}^{N_1\times N_2}}.$$

Based on the principles of Theorem 1, it follows that

$$L_\lambda(u) = -\min\left\{ f_1(\nu) + f_2(\zeta(\nu)) \;\middle|\; \nu \in (\mathbf{R}^9)^{N_1\times N_2} \right\}$$
$$= \min\left\{ f_1^*(-\xi(p)) + f_2^*(p) \;\middle|\; p \in (\mathbf{R}^3)^{N_1\times N_2} \right\},$$

where $p = \zeta(\nu)$. Based on the duality principle of definition 2, it yields $f_1^*(-\xi(p)) = \lambda_0||\xi(p)||_1$, and

$$f_2^*(p) = \max\left\{ \langle p, w\rangle_{(\mathbf{R}^3)^{N_1\times N_2}} - f_2(w) \;\middle|\; w \in (\mathbf{R}^3)^{N_1\times N_2} \right\}$$
$$= \max\left\{ \langle p, w\rangle_{(\mathbf{R}^3)^{N_1\times N_2}} - I_{\{||.||_\infty \le \lambda_1\}}(w) + \langle u, \zeta(w)\rangle_{\mathbf{R}^{N_1\times N_2}} \;\middle|\; w \in (\mathbf{R}^3)^{N_1\times N_2} \right\}.$$

Since $\zeta^* = -\delta$, it yields

$$f_2^*(p) = \max\left\{ \langle \delta(u), w\rangle_{(\mathbf{R}^3)^{N_1\times N_2}} - \langle p, w\rangle_{(\mathbf{R}^3)^{N_1\times N_2}} \;\middle|\; ||w||_\infty \le \lambda_1,\ w \in (\mathbf{R}^3)^{N_1\times N_2} \right\}$$
$$= \max\left\{ \langle \delta(u) - p, w\rangle_{(\mathbf{R}^3)^{N_1\times N_2}} \;\middle|\; ||w||_\infty \le \lambda_1,\ w \in (\mathbf{R}^3)^{N_1\times N_2} \right\}.$$

Choosing $k = \delta(u) - p$, it follows that

$$f_2^*(p) = \max\left\{ \sum_{s=1}^{2}\sum_{j=1}^{N_2}\sum_{i=1}^{N_1} w_s(i,j)\ k_s(i,j) \;\middle|\; ||w||_\infty \le \lambda_1,\ w \in (\mathbf{R}^3)^{N_1\times N_2} \right\}$$
$$\lambda_1\ ||\delta(u) - p||_1.$$

□

3.2 Primal-dual algorithm

This section contains the primal-dual algorithm described in [16] for solving (3). Primal-dual methods apply proximity operators, which can be defined for proper, lower semi-continuous, convex, and extended real-valued functions.

The followings are the proximity operators, which are used in this algorithm,

$$prox_{\tau F_1}(u) = \frac{u + \tau u_0}{1 + \tau},\ prox_{\tau F_2}(p) = p - \frac{p}{\max(\frac{|p|}{\tau\lambda_1}, 1)},$$

$$prox_{\sigma g}(\nu) = \frac{\nu}{\max(\frac{|\nu|}{\lambda_0}, 1)}.$$

Algorithm 1 to solve (3)

1. Set $k = 0$, choose parameters τ, σ, ρ, and the initial estimates $u^{(0)} \in \mathbf{R}^{N_1 \times N_2}$, $p^{(0)} \in (\mathbf{R}^3)^{N_1 \times N_2}$, $\nu^{(0)} \in (\mathbf{R}^9)^{N_1 \times N_2}$.
2. Calculate $u^{(k+1)}$, $p^{(k+1)}$ and $\nu^{(k+1)}$ using the following equations:
$P_1 := prox_{\tau F_1}(u^{(k)} - \zeta(\tau\zeta(\nu^{(k)})))$,
$P_2 := prox_{\tau F_2}(p^{(k)} + \tau\zeta(\nu^{(k)}))$,
$P_3 := prox_{\sigma g}(\nu^{(k)} + \sigma\ \xi(\delta(2\ p_1 - u^{(k)}) - (2\ p_2 - p^{(k)})))$,
$u^{(k+1)} := u^{(k)} + \rho\ (p_1 - u^{(k)})$,
$p^{(k+1)} := p^{(k)} + \rho\ (p_2 - p^{(k)})$,
$\nu^{(k+1)} := \nu^{(k)} + \rho\ (p_3 - \nu^{(k)})$.
3. Stop or set $k := k + 1$ and go back to step 2.

4 Numerical experiments

In this section, we test the performance of the proposed method on several sample images to remove noise (see Figure 2). Each image is corrupted by additive white Gaussian noise of standard deviation 0.18. We compare the new proposed method with the anisotropic TV, the isotropic TV, the upwind TV in [12], and the TGV method in [6] (see Figures 3,4,5,6,7,8,9,10,11,12,13,14 for the restored images). For the selection of the optimal regularization parameter, the algorithms corresponding to the anisotropic TV, the isotropic TV, the upwind TV, the TGV method, and the proposed method are implemented with many different choices for λ, and the λ value corresponding to the best peak signal to noise ratio (PSNR) (least relative error) is chosen as the optimal λ value.

Using the anisotropic TV, it performs well in removing noise but small details become unclear, and this TV scheme suffers from the staircasing effect, which appears as undesired patchy artifacts in slanted regions. The upwind TV has nice performance in preserving details but it has a remarkable drawback because some small white particles of noise will be remained in restored images, which indicates that the upwind TV is not capable of removing white noise. Moreover, the upwind TV suffers from the staircasing effect. The isotropic TV performs to some extent better than the anisotropic

TV and the upwind TV in noise removal but still some details are not reconstructed during the denoising process, and this TV scheme is not capable of alleviating the staircasing effect. Using the TGV method, it still suffers from the remaining of the staircasing effect, which indicates that it is not powerful enough to handle the severe noise. The proposed method outperforms the anisotropic TV, the isotropic TV, the upwind TV, and the TGV method both in the reconstruction of fine structures and the elimination of the staircasing effect. The numerical experiments illustrate that the new proposed method achieves higher quality in terms of PSNR and relative error (see Table 1). For example in the case of bird image, Table 1 illustrates that the proposed method achieves a PSNR value, which is about 0.187585 higher than the PSNR value of TGV model. If we notice the other quantities in Table 1, we observe that the PSNR value corresponding to the TGV model is about 0.129112 higher than the PSNR value corresponding to isotropic TV, and this PSNR difference is less than the PSNR difference of the proposed method and the TGV method.

The iteration numbers of optimization algorithm for both bird and bike images in each model is 1500. Figures 15,16,17, and 18 illustrate the PSNR and the relative error of various methods versus iteration numbers. For example, in the case of bike image, Figures 17 and 18 illustrate that after 600 iterations, the proposed method has smaller PSNR and higher relative error in comparison with the TGV model (TGV: PSNR=23.038355, Relative error=0.092436, proposed: PSNR=22.980077, Relative error=0.093058). If we increase the number of iterations to 1500, the TGV model achieves better quantities (TGV: PSNR=23.060928, Relative error=0.092196) in comparison with 600 iterations, and the proposed model achieves the best PSNR value (proposed: $PSNR = 23.080060$, Relative error=0.091993) in comparison with other methods. Even if we increase the iteration numbers again, very few changes are observed, and the proposed method will still have the best PSNR value and the least relative error in comparison with other methods.

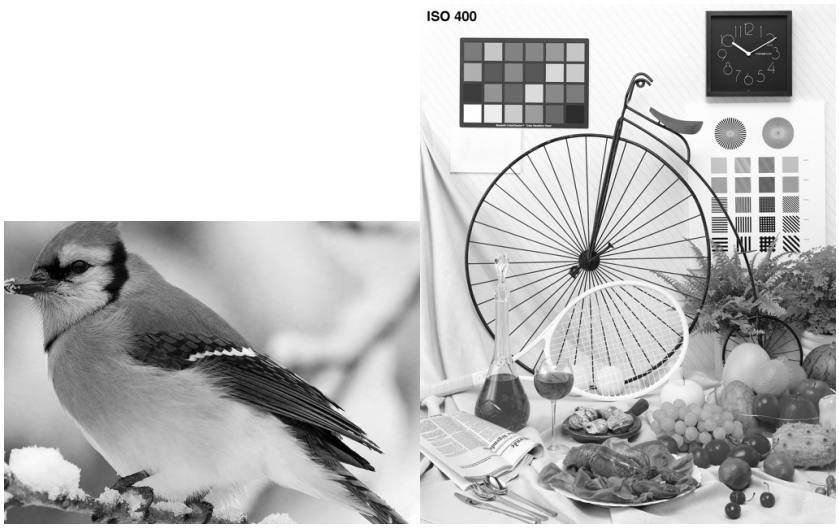

Figure 2: The test images used in our numerical experiments. Left: bird (490×674 in experiments); right: bike (640×512 in experiments).

Figure 3: From left to right: noisy bird image, restored bird image by anisotropic TV.

Figure 4: From left to right: restored bird images by isotropic TV and upwind TV.

Figure 5: From left to right: restored bird images by TGV and the new proposed method.

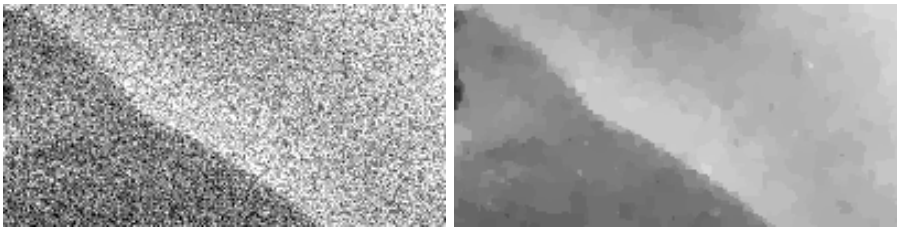

Figure 6: Zoomed-in regions of bird image. From left to right: noisy image, restored by anisotropic TV.

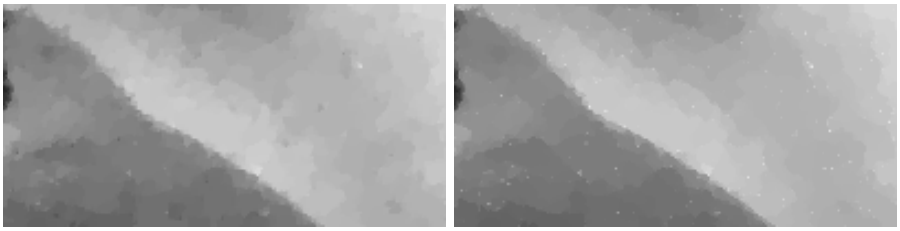

Figure 7: Zoomed-in regions of bird image. From left to right: restored by isotropic TV and upwind TV.

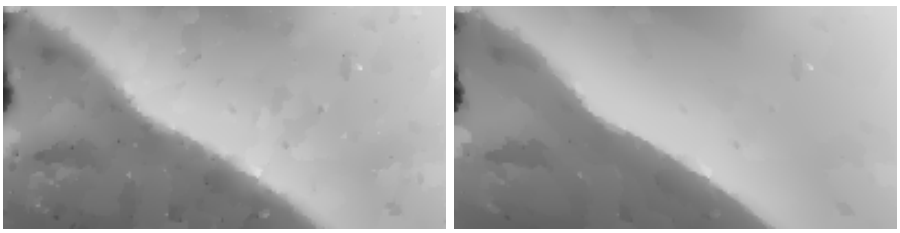

Figure 8: Zoomed-in regions of bird image. From left to right: restored by TGV and the new proposed method.

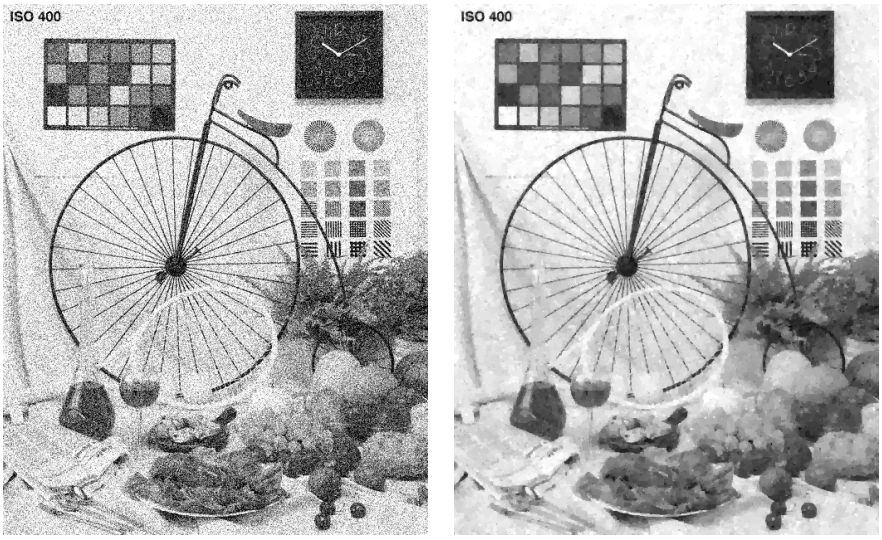

Figure 9: From left to right: noisy bike image, restored bike image by anisotropic TV.

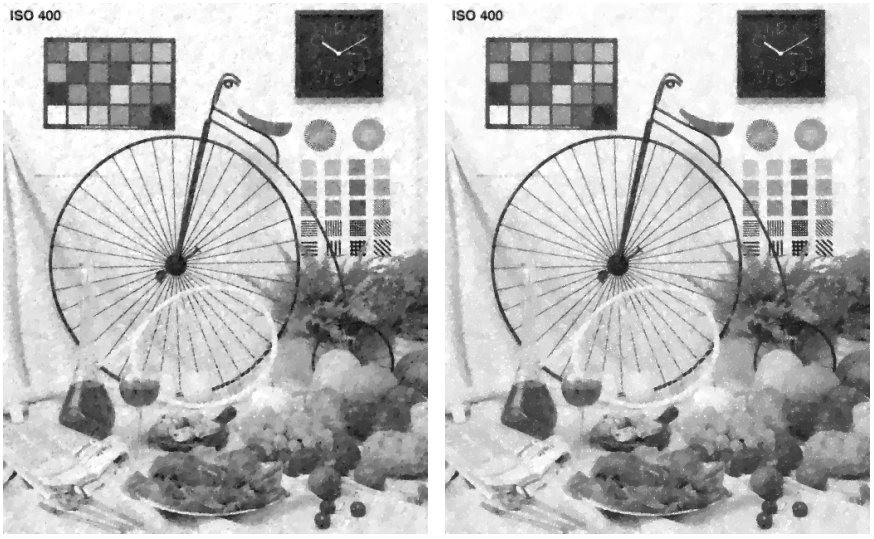

Figure 10: From left to right: restored bike images by isotropic TV and upwind TV.

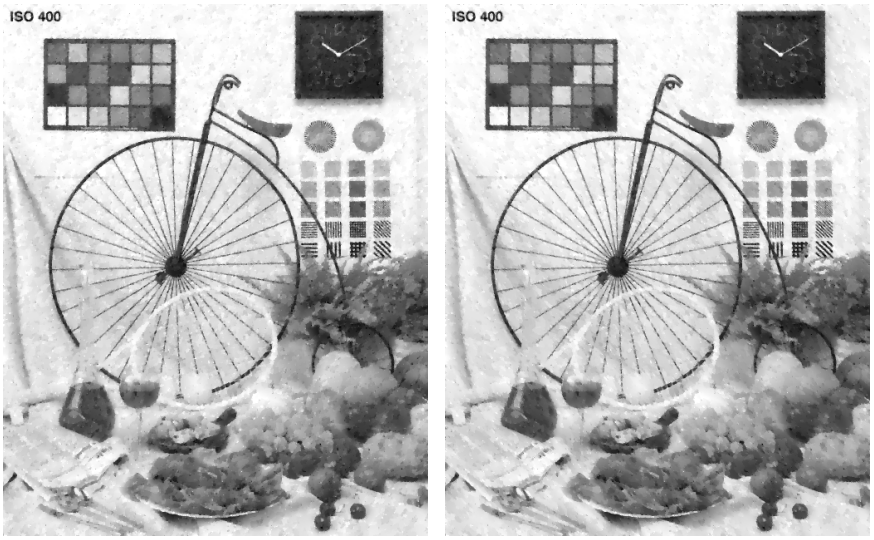

Figure 11: From left to right: restored bike images by TGV and the new proposed method.

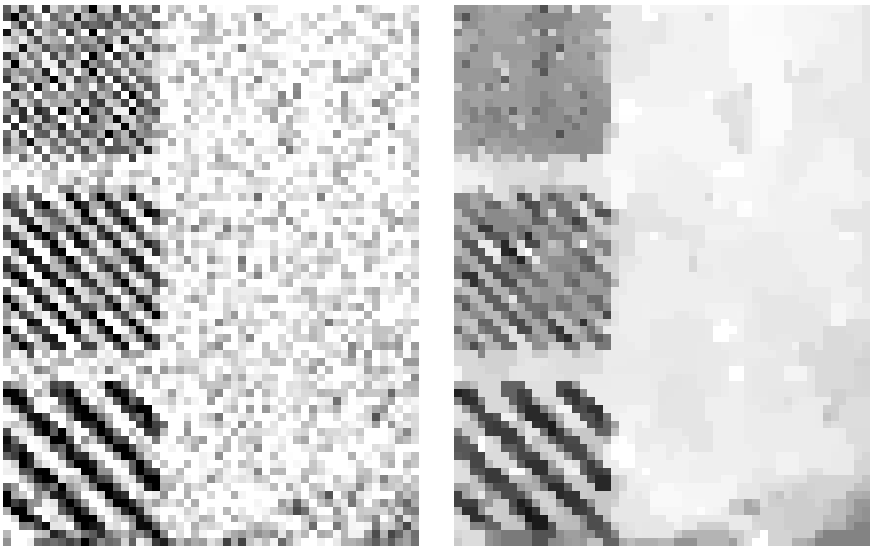

Figure 12: Zoomed-in regions of bike image. From left to right: noisy image, restored by anisotropic TV.

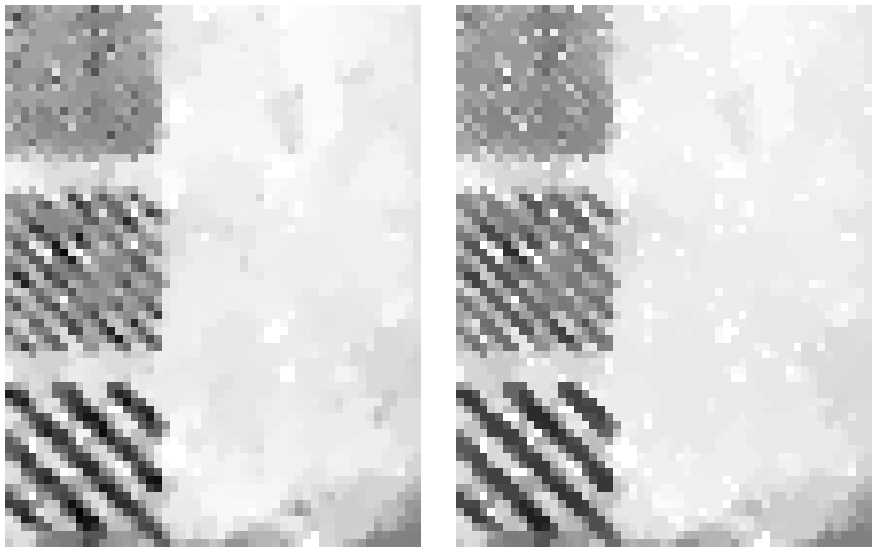

Figure 13: Zoomed-in regions of bike image. From left to right: restored by isotropic TV and upwind TV.

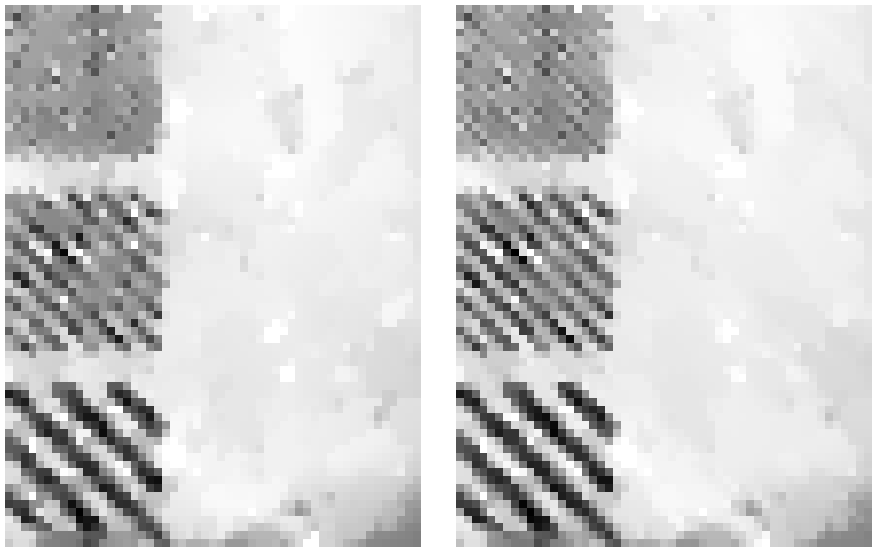

Figure 14: Zoomed-in regions of bike image. From left to right: restored by TGV and the new proposed method.

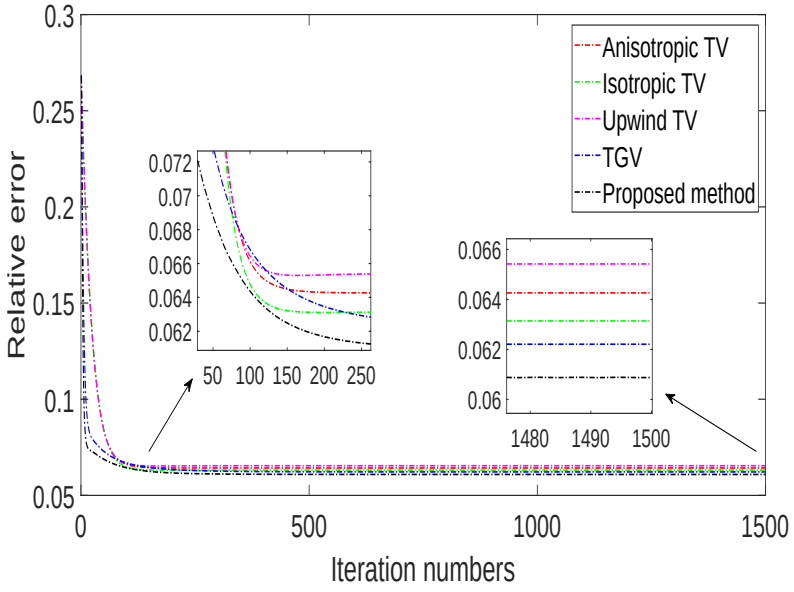

Figure 15: The sequence of relative error of bird image versus iteration numbers.

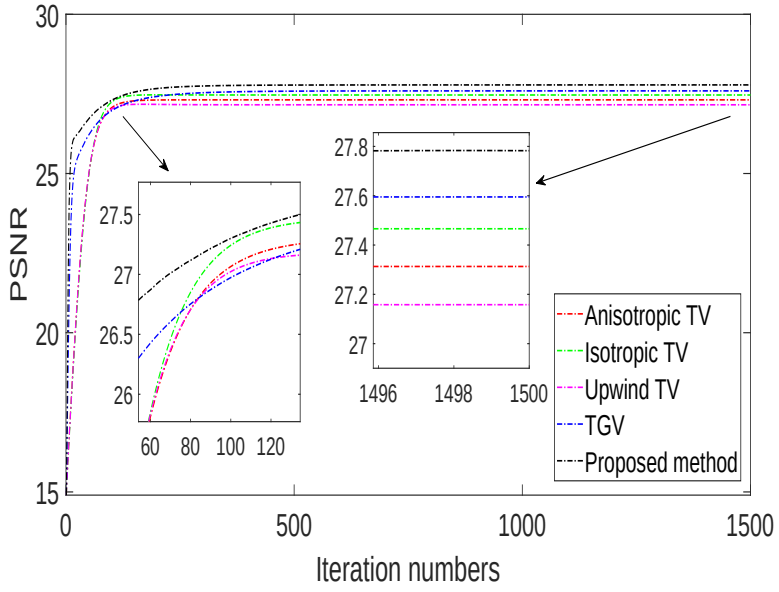

Figure 16: The sequence of PSNR of bird image versus iteration numbers.

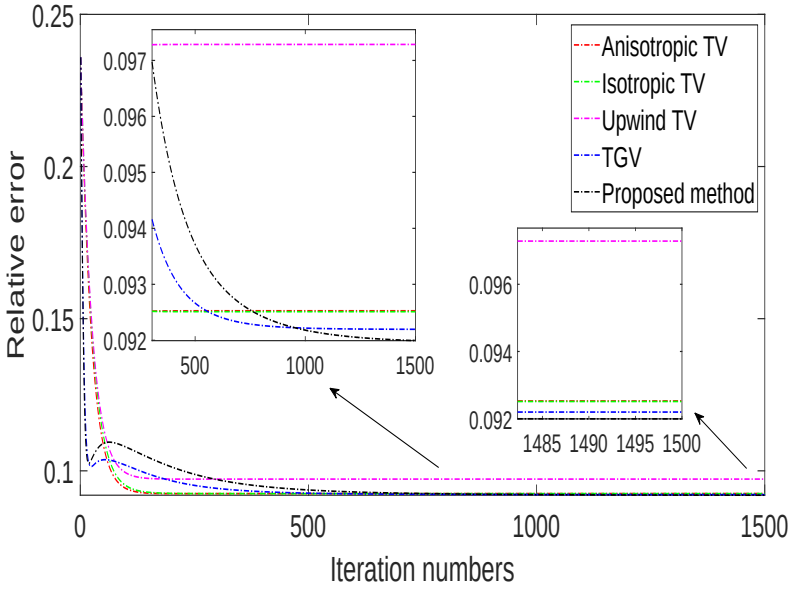

Figure 17: The sequence of relative error of bike image versus iteration numbers.

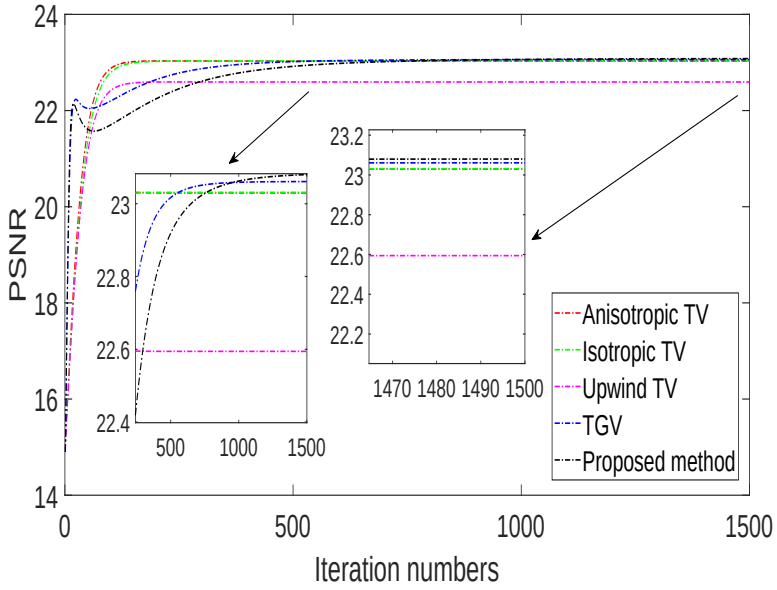

Figure 18: The sequence of PSNR of bike image versus iteration numbers.

Table 1: Performance comparison of restoration results in terms of relative error and the PSNR. The new proposed method achieves higher quality in terms of the PSNR and relative error.

Image	Method	Iterations	Optimal λ	Relative error	PSNR
Bird	Anisotropic TV	1500	0.14	0.064262	27.313069
Bird	Isotropic TV	1500	0.17	0.063141	27.466009
Bird	Upwind TV	1500	0.21	0.065420	27.158004
Bird	TGV	1500	(0.3, 0.16)	0.062209	27.595121
Bird	proposed	1500	(0.3, 0.13)	0.060880	27.782706
Bike	Anisotropic TV	1500	0.11	0.092527	23.029824
Bike	Isotropic TV	1500	0.13	0.092511	23.031338
Bike	Upwind TV	1500	0.155	0.097285	22.594246
Bike	TGV	1500	(0.21, 0.13)	0.092196	23.060928
Bike	proposed	1500	(0.14, 0.1)	0.091993	23.080060

5 Conclusion

This paper proposes to revisit the discreteTGV image denoising problem by redefining the operations via the inclusion of a diagonal term to reduce the staircasing effect, which is the patchy artifacts usually observed in slanted regions of the image. Numerical experiments confirm that the new proposed method achieves higher quality in terms of relative error and the PSNR compared with the conventional TGV method. The more direction analysis of first-order-derivative by using more oblique terms is considered as our future researches.

References

1. Aujol, J.F., Gilboa, G. and Papadakis, N. *Fundamentals of non-local total variation spectral theory*, In International Conference on Scale Space and Variational Methods in Computer Vision, Springer, Cham, (2015), 66–77.
2. Bauschke, H.H. and Combettes, P.L. *Convex analysis and monotone operator theory in Hilbert spaces*, Springer, New York, 2011.
3. Bioucas–Dias, J.M. and Figueiredo, M.A. *A new TwIST: Two-step iterative shrinkage/thresholding algorithms for image restoration*, IEEE Transactions on Image processing, 16(12) (2007), 2992–3004.
4. Blomgren, P. and Chan, T.F. *Color TV: total variation methods for restoration of vector-valued images*, IEEE transactions on image processing, 7(3) (1998), 304–309.

5. Blomgren, P., Chan, T.F., Mulet, P. and Wong, C.K. *Total variation image restoration: numerical methods and extensions*, In Proceedings of International Conference on Image Processing, IEEE, 3 (1997), 384–387.

6. Bredies, K., Kunisch, K. and Pock, T. *Total generalized variation*, SIAM Journal on Imaging Sciences, 3(3) (2010), 492–526.

7. Bredies, K. and Valkonen, T. *Inverse problems with second-order total generalized variation constraints*, Proceedings of SampTA 201 (2011).

8. Bresson, X. and Chan, T.F. *Fast dual minimization of the vectorial total variation norm and applications to color image processing*, Inverse problems and imaging, 2(4) (2008), 455–484.

9. Burns, M., Haidacher, M., Wein, W., Viola, I. and Groeller, E. *Feature emphasis and contextual cutaways for multimodal medical visualization*, In EuroVis, 7 (2007), 275–282.

10. Caselles, V., Chambolle, A. and Novaga, M. *The discontinuity set of solutions of the TV denoising problem and some extensions*, Multiscale modeling & simulation, 6(3) (2007), 879–894.

11. Caselles, V., Chambolle, A. and Novaga, M. *Regularity for solutions of the total variation denoising problem*, Revista Matematica Iberoamericana, 27(1) (2011), 233–252.

12. Chambolle, A., Levine, S.E. and Lucier, B.J. *An upwind finite difference method for total variation-based image smoothing*, SIAM Journal on Imaging Sciences, 4(1) (2011), 277–299.

13. Chan, T.F., Osher, S. and Shen, J. *The digital TV filter and nonlinear denoising*, IEEE Transactions on Image processing, 10(2) (2001), 231–241.

14. Chan, T.F. and Wong, C.K. *Total variation blind deconvolution*, IEEE transactions on Image Processing, 7(3) (1998), 370–375.

15. Chan, T.F., Yip, A.M. and Park, F.E. *Simultaneous total variation image inpainting and blind deconvolution*, International Journal of Imaging Systems and Technology, 15(1) (2005), 92–102.

16. Condat, L. *A primal-dual splitting method for convex optimization involving Lipschitzian, proximable and linear composite terms*, Journal of optimization theory and applications, 158(2) (2013), 460–79.

17. Elad, M. and Feuer, A. *Restoration of a single superresolution image from several blurred, noisy, and undersampled measured images*, IEEE transactions on image processing, 6(12) (1997), 1646–1658.

18. Fadili, J.M. and Peyr, G. *Total variation projection with first order schemes*, IEEE Transactions on Image Processing, 20(3) (2011), 657–669.

19. Georgiev, T.G. and Chunev, G.N. *Methods and apparatus for rendering output images with simulated artistic effects from focused plenoptic camera data*, U.S. Patent 8,665,341 (2014).

20. Guichard, F. and Malgouyres, F. *Total variation based interpolation*, In 9th European Signal Processing Conference, IEEE, (1998), 1–4.

21. Lou, Y., Zeng, T., Osher, S. and Xin, J. *A weighted difference of anisotropic and isotropic total variation model for image processing*, SIAM Journal on Imaging Sciences, 8(3) (2015), 1798–1823.

22. Nacereddine, N., Zelmat, M., Belaifa, S.S. and Tridi, M. *Weld defect detection in industrial radiography based digital image processing*, Transactions on Engineering Computing and Technology 2 (2005), 145–148.

23. Richardson, W.H. *Bayesian-based iterative method of image restoration*, Journal of the Optical Society of America, 62(1) (1972), 55–59.

24. Ring, W. *Structural properties of solutions to total variation regularization problems*, ESAIM: Mathematical Modelling and Numerical Analysis, 34(4) (2000), 799–810.

25. Rudin, L.I. and Osher, S. *Total variation based image restoration with free local constraints*, In Proceedings of 1st International Conference on Image Processing, IEEE, 1 (1994), 31–35.

26. Rudin, L.I., Osher, S. and Fatemi, E. *Nonlinear total variation based noise removal algorithms*, Physica D: nonlinear phenomena, 60(1-4) (1992), 259–268.

27. Santhanam, A.P., Fidopiastis, C.M., Hamza-Lup, F.G., Rolland, J.P. and Imielinska, C.Z. *Physically-based deformation of high-resolution 3D lung models for augmented reality based medical visualization*, MICCAI AMI-ARCS, (2004), 21–32.

28. Svakhine, N.A., Ebert, D.S. and Andrews, W.M. *Illustration-inspired depth enhanced volumetric medical visualization*, IEEE Transactions on Visualization and Computer Graphics, 15(1) (2009), 77–86.

29. Vogel, C.R. and Oman, M.E. *Fast, robust total variation-based reconstruction of noisy, blurred images*, IEEE transactions on image processing, 7(6) (1998), 813–824.

30. Wachs, J., Stern, H., Edan, Y., Gillam, M., Feied, C., Smith, M. and Handler, J. *A real-time hand gesture interface for medical visualization applications*, In Applications of Soft Computing, Springer, Berlin, Heidelberg, (2006), 153–162.

31. Zach, C., Pock, T. and Bischof, H. *A duality based approach for realtime TV-L1 optical flow*, In Joint Pattern Recognition Symposium, Springer, Berlin, Heidelberg, (2007), 214–223.

32. Zhang, D.D., Kong, W.K.A., You, J. and Wong, M. *Online palmprint identification*, IEEE Transactions on pattern analysis and machine intelligence, 25(9) (2003), 1041–1050.

33. Zhang, Z. and Blum, R.S. *Region-based image fusion scheme for concealed weapon detection*, In Proceedings of the 31st Annual Conference on Information Sciences and Systems, (1997), 168–173.